Preprints of the 19th World Congress
The International Federation of Automatic Control
Cape Town, South Africa. August 24-29, 2014

Dynamic Control of 3D Weld Pool Surface Based on Human Response Model

YuKang Liu*. YuMing Zhang*

**Institute for Sustainable Manufacturing and Department of Electrical and Computer Engineering, University of Kentucky, Lexington, KY, 40506, USA (Tel: 859-323-3322; e-mail: yuming.zhang@uky.edu).*

Abstract: Skilled human welders are so far the only to be capable of producing quality welds against perturbations. They adjust welding parameters based on their observation on 3D weld pool surface. Modelling their response to the 3D pool surface thus leads to next generation intelligent welding robots without human physical limitations. This paper first models this response as a human intelligence based controller. Its controlled process, with 3D pool surface as output and welding parameters as input in gas tungsten arc welding (GTAW), is then Hammerstein modelled in order to analyse its effectiveness. Analysis shows that this controller robustly controls the 3D pool surface under various perturbations. Closed-loop control welding experiments further validated this effectiveness. A foundation is thus established to rapidly transform skilled human welder's intelligence into robotic welding systems.

1. INTRODUCTION

GTAW (O'Brien, 1998) is the most widely used arc welding process for precision joining which typically requires a full penetration (Fig. 1) whose state is primarily specified by the back-side bead width w_b. While its control is an essential capability for next generation automated welding machines, its measurement typically requires top-side sensing methods due to the inconvenience in placing back-side sensors. The penetration state is thus not directly measured. To estimate, various top-side sensing techniques have been studied (Li and Zhang, 2001; Ma and Wei, 2010; Fan, Lv, and Chen, 2009; Song and Zhang, 2009), including pool oscillation, ultrasonic sensing, infrared sensing, and vision-based sensing method. Among all information which may be measured from the top-side, the weld pool surface may provide valuable insights into the weld penetration. In fact, skilled welders can successfully control the penetration state only based on their observation on the weld pool surface. Its scientific root is that the top-side and back-side weld pool surfaces must obey the volume constraint.

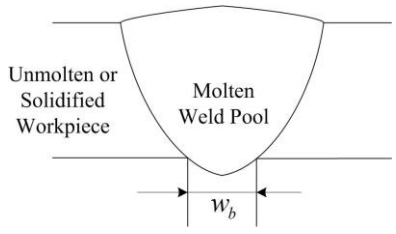

Fig.1 Weld pool and full penetration.

Monitoring weld pool surface is challenging due to the fluctuation of the liquid weld pool surface, being specular like a mirror, and the presence of the strong arc. The University of Kentucky is the first to make this realistic. A laser pattern was projected on the weld pool surface and the laser reflected from the specular surface was intercepted at a distance from the arc (Song and Zhang, 2009). While the reflected laser remains its intensity, the arc radiation reduces its intensity cubically with the distance. Clear images of the reflected laser can thus be obtained despite the strong arc. With the known incident rays of the projected laser and the surface continuity as a constraint, the reflection law has been used to analytically calculate the weld pool surface in real-time (Zhang, Wang, and Zhang, 2013).

However, to correlate/estimate the penetration state to/from any top-side measurements including the weld pool surface, models are needed. Empirical modelling has been studied to certain extent (Song and Hardt, 1994; Liu, Zhang, and Zhang, 2013; Liu and Zhang, 2013). Unfortunately, for the most promising top-side measurement (3D weld pool surface), success in empirical modelling has been limited. Numerical models (Traidia and Roger, 2011; Mougenot, Gonzalez, Freton and Masquere, 2013) may be promising, yet their extensive calculations needed restricted their application in real-time monitoring and control.

Skilled human welders can adjust the welding parameters to produce quality welds for desired penetration implies (1) they can derive the penetration state from the weld pool surface and (2) they can successfully adjust the welding parameters based on the weld pool surface as the feedback. Hence, a skilled human welder naturally executes a model that correlates the penetration state to the weld pool surface and an algorithm to determine how to adjust the welding parameters per the weld pool surface as feedback. However, the model and feedback control algorithm are combined as a human response model whose outputs are the welding parameters (inputs of the controlled process) and inputs are the parameters which characterize the weld pool surface (outputs of the controlled process).

As such, the authors propose to control the weld pool surface based on human welder response model. The estimation model unavailability and control algorithm design issues are both resolved. The resultant robotic control system may produce quality welds like a skilled welder without their

physical limitations (inconsistent concentration, fatigue, stress). To verify the effectiveness of the human welder response model based control, its effect on the welding process under various conditions needs to be studied. To this end, weld pool surface as a dynamic process with welding parameters as the inputs needs to be modelled.

The authors have established a linear state space model to correlate the weld pool surface as specified by their characteristic variables to the inputs of the welding process (Zhang, Liu, Wang, and Zhang, 2012; Liu and Zhang, 2013). However, the fundamental nonlinear characteristic as will be demonstrated in this paper is not comprehensively represented. Hammerstein model, on the other hand, is considered an effective method to model nonlinear dynamics (Zhao, 2010; Cai and Bai, 2011) for many practical systems. Hence, this paper will Hammerstein model the weld pool surface and use the resultant model to analyse the human welder response model based control proposed.

In Section 2, response of a skilled human welder to 3D weld pool surface will be modelled using Adaptive Neuro-Fuzzy Inference System (ANFIS). Then the weld pool surface specified by its characteristic variables will be Hammerstein modelled in Section 3. In Section 4, the proposed control system for 3D weld pool surface based on human welder response model will be analysed revealing the robustness of the system against perturbations. Control experiments are thus then conducted to further verify the effectiveness of the proposed control system in Section 5. Conclusions are finally drawn in Section 6.

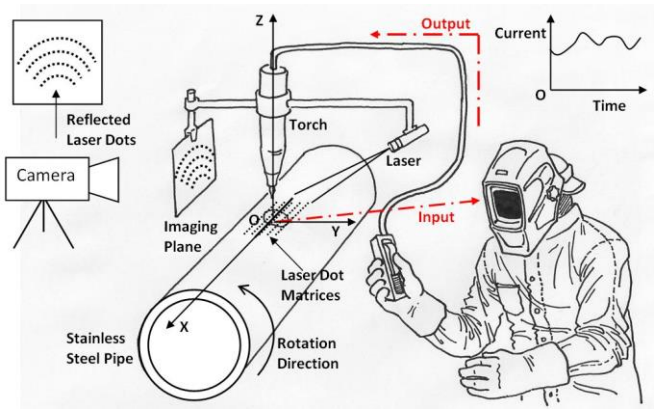

Fig.2 Manual control system of GTAW process (Liu, Zhang, and Kvidahl, 2014).

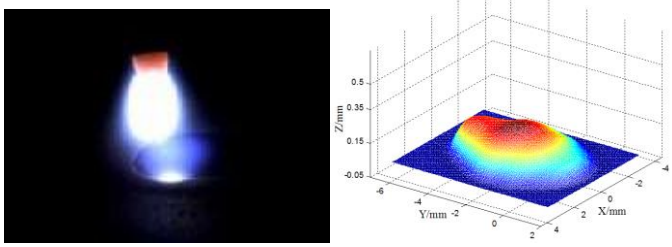

Fig.3 GTAW weld pool. Left: pool Image; right: reconstructed pool surface (Liu and Zhang, 2013).

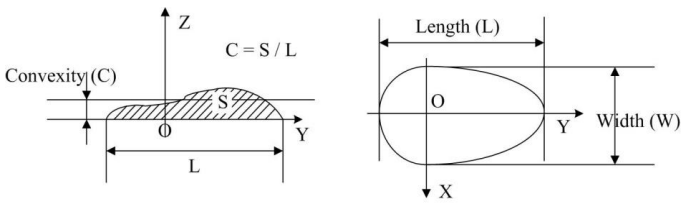

Fig.4 Illustration of weld pool characteristic parameters (Liu and Zhang, 2013).

2. MODELING SKILLED HUMAN WELDER RESPONSE

2.1 Experimental System

A manual control system (Liu, Zhang, and Zhang, 2013) is developed combining the 3D weld pool sensing system with a manual control mechanics (Fig.2). In this system a skilled human welder holds the current regulator while observing the weld pool surface and adjusts the welding current accordingly in an effect to produce desired full penetration. The pipe weld application is made using the Direct-Current Electrode-Negative GTAW. The material of the pipe is stainless steel 304. The outer diameter and wall thickness of the pipe are 113.5mm and 2.03 mm, respectively. The pipe rotates during experiment while the torch stays stationary. The rotation speed and motion of torch are controlled by a computer to achieve required welding speed and arc length. In the sensing system, a 20mw illumination laser generator projects a 19-by-19 dot matrix structured light pattern on the weld pool region. Part of the dot matrix projected on the weld pool is reflected by the specular mirror-like weld pool surface which has been distorted by the arc pressure. An imaging plane is installed with a distance about 100 mm from the torch. A camera is located behind the imaging plane directly aiming at it. Since the reflected laser remains its intensity while the arc radiation reduces cubically, reflected laser (in milliwatts) dots are clearly imaged on an imaging plane while the arc (in kilowatts) is not. By using specific image processing and 3D reconstruction scheme (Zhang, Wang and Zhang, 2013), the 3D weld pool surface can be reconstructed in milliseconds which is considered truly real-time (see Fig. 3 for a weld pool image and reconstructed weld pool surface). Fig.4 shows the illustration of the variables which characterize the weld pool surface. After the weld pool boundary is acquired, the weld pool width and length can be calculated straightforwardly. The convexity is defined as the intercepted area divided by the length of the weld pool (i.e., the average height of the weld pool surface).

Nine dynamic experiments are conducted with the welding speed to vary within reasonable ranges in order to change the weld pool surface. Then the skilled welder adjusts the current to try to maintain the same penetration state despite the changed welding speed. During experiments, the characteristic variables of the 3D weld pool surface are recorded together with the adjustments in the current.

2.2 Modelling Human Welder Response

It is found that the welder response can be modelled as

$$\Delta I(k)=f(W_f(k-3),L_f(k-3),C_f(k-3),\Delta I(k-1)) \qquad (1)$$

where W_f, L_f, C_f are the low-pass filtered weld pool width, length, and convexity measurements, respectively. The sampling period in the model is 0.5 s because the human welder is found to scan the weld pool approximately at 2Hz. The delay, 3 periods or 1.5 s, is estimated from step response experiments and should be a result of the neuromuscular and central nervous latencies.

The simplest form from (1) can be expressed by

$$\Delta I(k)=\alpha_1 W_f(k-3)+\alpha_2 L_f(k-3)+\alpha_3 C_f(k-3)+\alpha_4 \Delta I(k-1) \quad (2)$$

Using the standard least squares algorithm this linear model can be fitted from the experimental data:

$$\begin{aligned}\Delta I(k)=&-0.16W_f(k-3)-0.082L_f(k-3)\\&+1.81C_f(k-3)+0.26\Delta I(k-1)\end{aligned} \quad (2A)$$

As a human inference mechanism, the human welder response should inevitably be fuzzy and nonlinear. However, the abstract thoughts or concepts in human reasoning are difficult to extract from the domain knowledge. In neuro-fuzzy modelling, abstract thoughts or concepts in human reasoning are incorporated with numerical data so that the development of fuzzy models becomes more systematic and less time consuming. In this study, a neuro-fuzzy modelling technique, ANFIS (Jang, 1993), is used to model skilled human welder response represented by Equation (1).

The fuzzy input variables are partitioned by 2. The resultant model root mean square error (RMSE) and average model error are listed in Table I. Both criteria are improved by the proposed ANFIS model. One may think that the model improvement from Table I (4% to 7% for two criteria used in this study) is not significant. However, ANFIS model is derived in analytical form and can be implemented in real-time. The resultant model improvement is achieved at no additional costs. In addition, the human welder response is better modelled and understood. In this sense, the ANFIS model is considered a better way to represent the intrinsic nonlinear and fuzzy inference human welder possesses.

3. MODELING 3D WELD POOL SURFACE

In Hammerstein model (Fig.5) a static input nonlinearity is followed by a linear dynamical part. Various static experiments have been first carried out. Results show that for the width and length, incorporating nonlinearity does not improve the fitting results significantly. For the convexity, nonlinearity does provide significant improvements. The identified nonlinear static model for the convexity (mm) is:

$$C_n = 1.36u_1 - 0.09u_1^2 + 4.75u_2 - 1.53u_2^2 - 0.31u_1u_2 - 6.17 \quad (3)$$

where $u_1 = I/10$ and $u_2 = 1/\sqrt{s}$ with I and s being the welding current (A) and speed (mm/s), respectively. The affined inputs to be inputted into the convexity model can thus be defined as:

$$\begin{cases} v_1 = 1.36u_1 - 0.09u_1^2 - 0.31u_1u_2 \\ v_2 = 4.75u_2 - 1.53u_2^2 - 6.17 \end{cases} \quad (4)$$

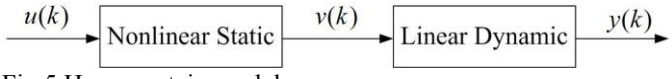

Fig.5 Hammerstein model.

Thirteen dynamic experiments have been conducted in order to obtain data to model the complex correlation between the welding process inputs (welding current and speed) and 3D weld pool surface characterized by its width, length, and convexity. It is observed that the weld pool surface varies substantially resulting from fluctuations of the welding current and speed. Specifically, the ranges for the weld pool width, length, and convexity are [1 mm, 6.42 mm], [1.2 mm, 6.9 mm], and [0.05 mm, 0.27 mm], respectively. Modelling trails reveal that linear models have noticeable fitting errors which can be improved by incorporating nonlinear factors representing the cross-coupling between three weld pool parameters.

The following models are thus proposed for the width, length, and convexity, respectively:

$$\begin{aligned}W(k)=&\sum_{j=1}^{2}\alpha_W(j)W(k-j)+\sum_{j=1}^{2}\beta_W(j)u_1(k-j)\\&+\sum_{j=1}^{3}\gamma_W(j)u_2(k-j)+c_W+NF_W\end{aligned} \quad (5A)$$

$$\begin{aligned}L(k)=&\sum_{j=1}^{2}\alpha_L(j)L(k-j)+\sum_{j=1}^{3}\beta_L(j)u_1(k-j)\\&+\sum_{j=1}^{6}\gamma_L(j)u_2(k-j)+c_L+NF_L\end{aligned} \quad (5B)$$

$$\begin{aligned}C(k)=&\sum_{j=1}^{2}\alpha_C(j)C(k-j)+\sum_{j=1}^{3}\beta_C(j)v_1(k-j)\\&+\sum_{j=1}^{3}\gamma_C(j)v_2(k-j)+c_C+NF_C\end{aligned} \quad (5C)$$

where $\alpha_P, \beta_P, \gamma_P, c_P, NF_P, P = [W, L, C]$ are the parameters to be identified. NF_Ps are the residuals of the model and account for the cross-coupling between three weld pool

TABLE I. MODEL COMPARISON BETWEEN NEURO-FUZZY MODEL AND LINEAR MODEL

	Average Model Error (A)	RMSE (A)
Linear Model	0.52	0.79
ANFIS Model	0.50	0.76

TABLE II. WELD POOL MODEL PARAMETERS

	α_P	β_P (mm/A)	γ_P ($mm\sqrt{mm/s}$)	c_P (mm)
Width	[0.802 0.099]	[0.19 -0.054]	[0.029 0.386 0.131]	-0.941
Length	[0.708 0.187]	[0.06 -0.01 0.001]	[-0.039 -0.581 0.416 -0.338 0.516 -0.041]	0.231
Convexity	[0.584 0.201]	[-0.006 0.002 0.001]	[-0.014 -0.001 0.012]	0.071

TABLE III. WELD POOL MODEL ERRORS

	Average Model Error (mm)	RMSE (mm)
Width	0.1797	0.2326
Length	0.2218	0.2929
Convexity	0.0114	0.0147

characteristic parameters. The model orders are selected by evaluating the RMSE. ANFIS technique (Jang, 1993) is utilized to model the residuals NF_P with other two pool parameters at the current instant. The identified model parameters are listed in Table II, and the obtained model errors are shown in Table III.

The steady state models for the width, length, and convexity can be derived from equation (5A)-(5C) together with parameters specified in Table II:

$$W = 1.36u_1 + 5.46u_2 - 9.41 \quad (6A)$$

$$L = 0.486u_1 - 0.638u_2 + 2.2 \quad (6B)$$

$$C = -0.0152u_1 - 0.0152u_2 + 0.36 \quad (6C)$$

For the weld pool width, the static gains for $u_1 = I/10$ and $u_2 = 1/\sqrt{s}$ are 1.36 mm/A and 5.46 $mm\sqrt{mm/s}$, respectively. This makes sense because an increase in the welding current and a decrease in the welding speed should both increase the heat input into the weld pool and the pool width. For the weld pool length, increasing the welding current also increases the heat input, yet the increasing rate is not as significant as the width (0.486 mm/A compared to 1.36 mm/A). When the welding speed is decreased, the length is supposed to decrease with a negative coefficient of -0.638 $mm\sqrt{mm/s}$. This is understandable because the increase of the speed causes the weld pool to elongate as the dragging effect. For the convexity, increasing the welding current and decreasing the welding speed are likely to decrease the weld pool convexity with both coefficients being -0.0152 mm/A. The linear model (6C) might not be sufficient in understanding this complex nonlinear relationship. Fig. 6 plots the model calculated width, length, and convexity for 4 cases of welding speeds (1mm/s, 1.2mm/s, 1.4mm/s and 1.6mm/s) when the welding current increases from 56 A to 68A. For the weld pool width, as the welding current increases, the width also increases. For a given welding current, an increase in the welding speed implies a decrease in the weld pool width. This coincides with our analysis on the steady state model (6A). For the weld pool length, as the current increases, the length becomes larger. For a given welding current, an increase in the welding speed increases the length. This observation also agrees with our previous analysis. The nonlinear correlation between the convexity and welding process inputs is depicted in Fig. 6. For small welding speed (e.g. 1 mm/s), as the welding current increases, the pool convexity firstly increases, then starts to decrease. Actually when the current increases, more metals are melted, resulting in larger convexity. However, as the current becomes larger, the increase in the arc pressure becomes the dominant factor. The pool becomes more concave and the penetration becomes deeper. Thus, the pool convexity starts to decrease. Similar phenomena occur for other welding speeds, while the dominant factor might be different for different welding currents. The increasing rates for different welding speeds are also different as opposed to the linear models for the width and length (shown in Fig. 6). It is apparent that these nonlinear models play an important role in accurately modelling the weld pool surface and understanding this complex correlation.

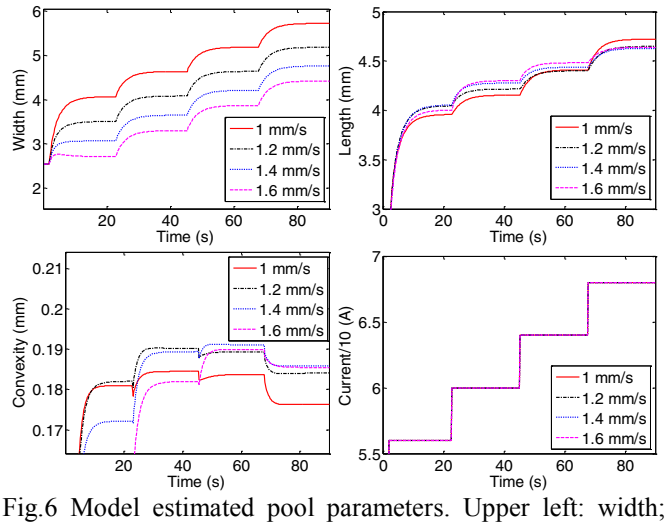

Fig.6 Model estimated pool parameters. Upper left: width; upper right: length; lower left: convexity; lower right: current.

4. SYSTEM ANALYSIS

The system schematic is illustrated in Fig. 7. Skilled human response model (1) constructed in Section 2 outputs the current adjustment and the adjustment is applied to the 3D weld pool surface model described in Section 3. This 3D weld pool surface model outputs the estimated weld pool surface by its width, length, and convexity which are then inputted into the welder response model. Fig. 8 depicts the system response when the welding speed is 1.0 mm/s with initial currents ranging from 52A to 58A. It is observed that despite the difference in the initial current, the system converges to steady state with 63.7A steady state welding current. As the initial current approaches the current steady

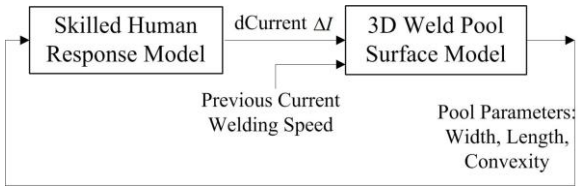

Fig.7 System schematic.

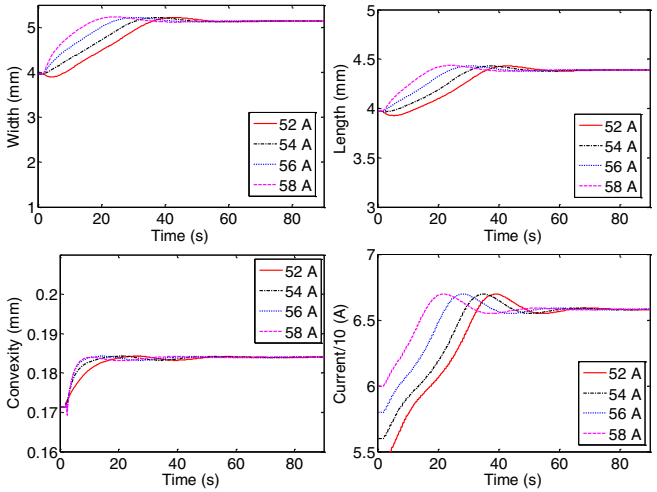

Fig.8 System response for speed=1.0 mm/s. Upper left: width; upper right: length; lower left: convexity; lower right: current.

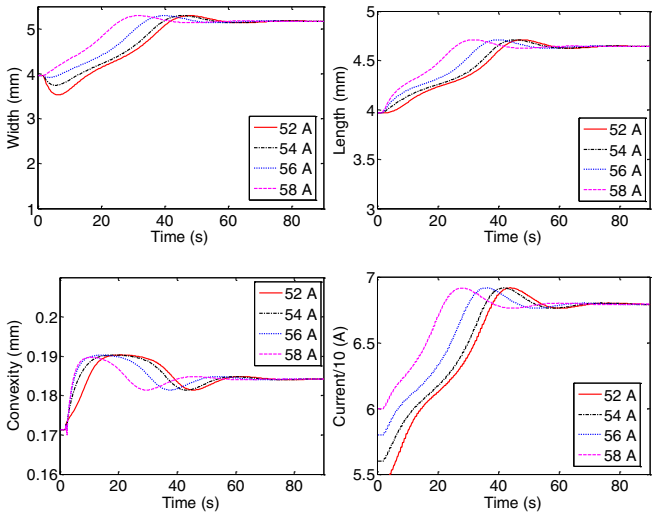

Fig.9 System response for speed=1.2 mm/s. Upper left: width; upper right: length; lower left: convexity; lower right: current.

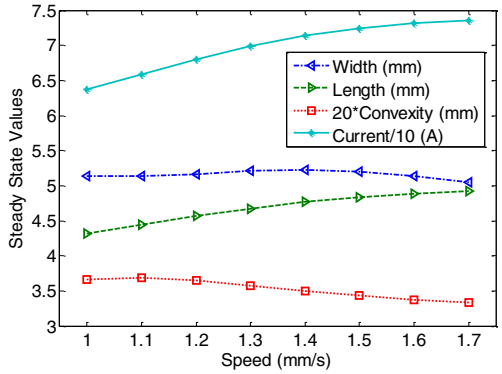

Fig.10 Steady state values versus welding speeds.

state value, the convergence time becomes shorter. The width, length, and convexity converge to 5.14mm, 4.32mm, and 0.18mm, respectively. The robustness of the system against initial current variation is thus verified. Fig. 9 depicts the system response when the welding speed is 1.2 mm/s to verify the robustness again. Compared to Fig. 8, the system takes longer time to converge, and the current steady state value is 67.96A. This makes sense because an increase in the welding speed decreases the heat input, and the human welder (response model) should increase the current in order to maintain the needed penetration. The robustness of the system against welding speed is thus also demonstrated. Fig. 10 shows the system steady state values with respect to different welding speeds. Since the process model changes with the welding speed and the welder only adjusts the welding current to control the penetration rather than the characteristic parameters, their steady-state values change with the welding speed. When the speed is slow, the pool width could be slightly greater than the length. This may be due to heat transfer condition difference in two directions.

5. CONTROL EXPERIMENTS

The developed closed-loop control system is illustrated in Fig. 11. A computer connected to the camera processes the captured image, reconstructs the weld pool surface, and extracts three characteristic variables in real-time. The skilled human intelligence model then outputs the current. In the first experiment, the arc length and welding speed are set at 5 mm and 1 mm/s, respectively. The experimental results are given in Fig.12-14. The process begins with an open-loop period (about 38 s - period A with initial current 52A), which brings the back-side bead width to about 3 mm. In first 42 s after period A, no error exists between the calculated current and applied current. The skilled human welder model is able to control the back-side bead width to about 5 mm (Fig. 14) by increasing the current to about 62 A (Fig. 13). In t = 103 s, the current disturbance is applied. The welding current is set at 50A, which is about 12A smaller than the calculation. The welder model adjusts the current to about 61 A in an effect to

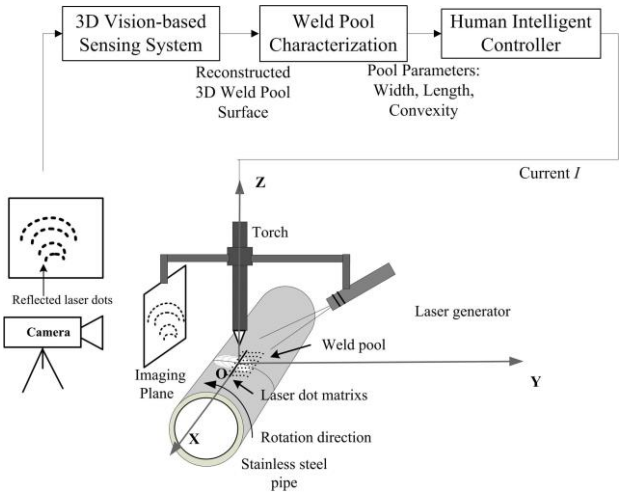

Fig.11 Illustration of the closed-loop control system.

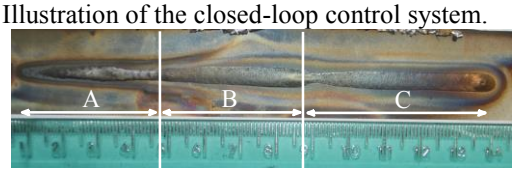

Fig.12 Back-side weld for current disturbance experiment.

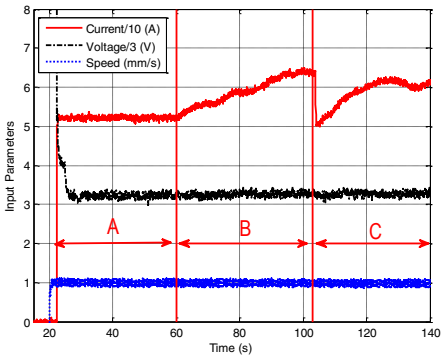

Fig.13 Control signals for current disturbance experiment.

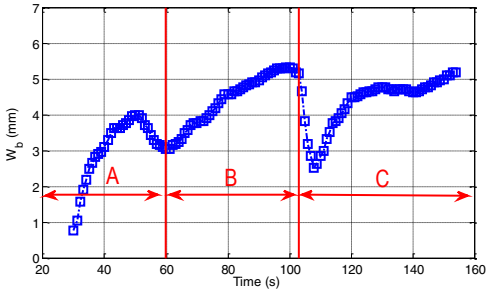

Fig.14 Offline measured back-side bead width for current disturbance experiment.

compensate this artificial current disturbance (Fig. 13) such that the back-side bead width be maintained around 5 mm. The controller's robustness against welding current disturbance is thus verified. In the second experiment, a step change in the welding speed is applied. The results are shown in Fig. 15 to 16. After an open-loop period (A), the controller is applied. The speed changes from 1mm/s in the first control period (B) to 1.1 mm/s in the second control period (C). The weld pool width and length immediately decrease, while the weld pool convexity increases due to the step speed change. The controller adjusted the current from 58 A to about 60A.

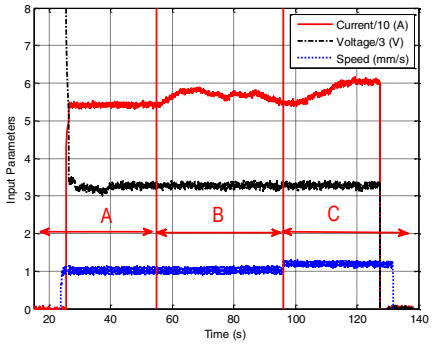

Fig.15 Control signal in speed change experiment.

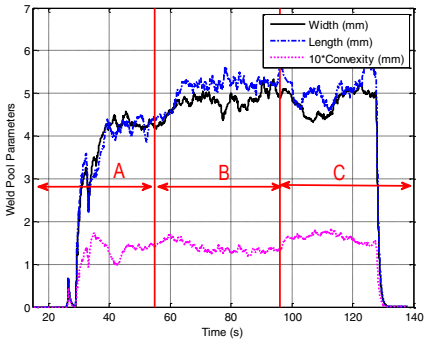

Fig.16 Pool surface parameters in speed change experiment.

6. CONCLUSIONS

Controlling 3D weld pool surface based on human welder response model possesses two major advantages: ability to control the weld penetration despite unavailability of the penetration estimation model and ability to facilitate rapid design of control algorithm. The identified nonlinear 3D weld pool surface model facilitated the ability to analyse the effectiveness of the human welder response based controller. Analysis and welding experiments both verified the effectiveness of this human welder response model based control system against perturbations.

ACKNOWLEDGEMENT

This work is funded by the National Science Foundation under grant CMMI-0927707 and IIS-1208420.

REFERENCES

Cai, Z. and Bai, E.W. (2011) Making parametric hammerstein system identification a linear problem. *Automatica* vol. 47(8), pp. 1806 – 1812.

Fan, C.L., Lv, F. and Chen, S. (2009) Visual sensing and penetration control in aluminum alloy pulsed GTA welding. *International Journal of Advanced Manufacturing Technology*, vol. 42 (1), pp. 126-137.

Jang, J.S.R. (1993) ANFIS: Adaptive-network-based Fuzzy Inference Systems. *IEEE Transactions on Systems, Man, and Cybernetics*, vol. 23(3), pp.665-685.

Li, P.J. and Zhang, Y.M. (2001) Precision Sensing of Arc Length in GTAW Based on Arc Light Spectrum. *Journal of Manufacturing and Science Engineering*, vol. 123, pp. 62-65.

Liu, Y.K. and Zhang Y.M. (2013) Control of 3D weld pool surface. *Control Engineering Practice*, vol. 21(11), pp. 1469-1480.

Liu, Y.K., Zhang, Y.M. (2013) Model-based Predictive Control of Weld Penetration in Gas Tungsten Arc Welding, *IEEE Transactions on Control Systems Technology*, vol. PP(99), pp. 1-12.

Liu, Y.K., Zhang, W.J., Zhang, Y.M. (2013) Dynamic neuro-fuzzy based human intelligence modeling and control in GTAW, *IEEE Transactions on Automation Science and Engineering*, in press.

Liu, Y.K., Zhang, W.J., Zhang, Y.M. (2013) Estimation of Weld Joint Penetration Under Varying GTA Pools, *Welding Journal*, vol. 92(11), pp. 313s-321s.

Liu, Y.K., Zhang, Y.M., Kvidahl, L. (2014) Skilled Human Welder Intelligence Modeling and Control: Part I-Modeling, *Welding Journal*, vol. 93, pp. 46s-52s.

Ma, H.B., and Wei, S.C. (2010) Binocular vision system for both weld pool and root gap in robot welding process. *Sensor Review*, vol. 30(2), pp. 116-123.

Mougenot J., Gonzalez, P., Freton, J.J., and Masquere, M. (2013) Plasma–weld pool interaction in tungsten inert-gas configuration. *Journal of Physics. D: Applied Physics*. vol. 46, pp. 135206.

O'Brien R. (1998) *Welding Handbook, 8th Edition vol. 2 – Welding Processes*. AWS, Miami, FL.

Song, H.S. and Zhang, Y.M. (2009) Error analysis of a three-dimensional GTA weld pool surface measurement system. *Welding Journal*. vol. 88(7), pp. 141–148.

Song J.B. and Hardt D.E. (1994) Dynamic modeling and adaptive control of the gas metal arc welding process. *ASME Journal of Dynamics Systems, Measurement, and Control*, vol. 116(3), pp. 405-410.

Traidia A. and Roger F. (2011) Numerical and experimental study of arc and weld pool behaviour for pulsed current GTA welding. *International Journal of Heat and Mass Transfer*, vol. 54, pp. 2163–2179.

Zhang, W.J., Liu, Y.K., Wang, X., Zhang, Y.M. (2012) Characterization of three-dimensional weld pool surface in Gas Tungsten Arc Welding", *Welding Journal*. vol. 91, pp. 195s-203s.

Zhang, W., Wang, X., Zhang, Y. (2013) Analytical real-time measurement of a three-dimensional weld pool surface, *Measurement Science and Technology*, vol.24, 115011 (18pp).

Zhao, W.X. (2010) Parametric identification of hammerstein systems with consistency results using stochastic inputs. *IEEE Transactions on Automatic Control* vol. 55(2), pp. 474–480.